



Ultrastrong behaviors of a non-equiautomic Ti-Zr-Ni-Cu-Be high entropy metallic glass with ultrahigh glass forming ability



Yuanyuan Wang ^{a,b,c}, Zhengwang Zhu ^{a,b,c,*}, Aimin Wang ^{a,b,c}, Haifeng Zhang ^{a,b,c}

^a Shi-changxu Innovation Center for Advanced Materials, Institute of Metal Research, Chinese Academy of Sciences, Shenyang 110016, China

^b CAS Key Laboratory of Nuclear Materials and Safety Assessment, Institute of Metal Research, Chinese Academy of Sciences, Shenyang 110016, China

^c School of Materials Science and Engineering, University of Science and Technology of China, Shenyang 110016, China

ARTICLE INFO

Keywords:

High-entropy metallic glass
Thermodynamics
Kinetics
Fragility
Glass-forming ability

ABSTRACT

We studied the thermodynamics and kinetics of a non-equiautomic $Ti_{32.8}Zr_{30.2}Ni_{5.3}Cu_9Be_{22.7}$ high entropy metallic glass (HEMG, $\Delta S_{config} \sim 1.44R$) with a critical size for glass formation over 50 mm. The characteristic transition temperature, enthalpy of transition and specific heat capacity along with the relaxation time at different heating rate were determined using differential scanning calorimeter (DSC) measurements. It reveals that the present HEMG supercooled liquid shows the lowest thermodynamic driving force against the nucleation and growth of crystalline phases with comparing to other typical MG formers. Meanwhile, it exhibits the ultrastrong behavior near glass transition in terms of the Angell's fragility concept. The alloy has a fragility index of $D^* = 45.2$, higher than all the typical MG formers reported so far. Both thermodynamic and kinetic factors are responsible for the ultrahigh glass-forming ability of the HEMG alloys.

1. Introduction

High entropy alloy (HEA) has been a novel concept of alloy design referring to the alloy containing at least five components of the equiautomic or near-equiautomic ratio of 5~35% in the last few decades [1]. Some unique properties were reported for HEAs, for examples, the trade-off of strength and ductility, high toughness in the cryogenic temperature, etc., due to high configurational entropy (ΔS_{config}), sluggish diffusion and severe lattice distortion, etc. [2~5]. Similarly, some HEAs with amorphous structure also exhibited intriguing properties [6~15]. It is indicated that metastable engineering would become a useful strategy to design novel HEAs with high performance.

The alloys with amorphous structure called metallic glasses (MGs) have been widely investigated for serval decades as prospective candidates for engineering structural materials. However, the lack of tensile plasticity at room temperature significantly limits their practical applications [16~18]. High entropy MGs (HE-MGs) will be a probability to overcome the aforementioned bottleneck issue based on the following two points. The first one is HE-MGs contain multi-components, which agree with the important criterion for glass formation named "the confusion principle" [19], promoting the glass formation upon solidification. The second one is the existence of wider composition space to be

exploited where the alloy with the specific composition will show the unique properties, i.e., the tensile plasticity and outstanding functional properties, etc.. Very recently, some HE-MGs were fabricated in the Ca-Mg-Yb-Sr-Zn [7], RE-Ni/Co/Fe-Al (RE referring to the rare element) [8], Fe-Co-Ni- (Si, B, P and C) [13], Pd-Pt-Ni-Cu-P [9], Ti-Zr-Hf-Cu/Ni-Be [10~12], alloys. Although these HE-MGs exhibit some unique physical and chemical properties, the glass-forming ability (GFA) of these alloys was not as high as expected, most of which can only be cast into the full amorphous samples with a diameter of several millimeters. The forming mechanism of HE-BMGs needs particularly intensive investigation in order to develop some HE-MGs with not only interesting performance but also high GFA.

Tang et al. developed Ti-Zr-Ni-Cu-Be HE-MG with a maximum diameter greater than 50 mm by optimizing the composition [6]. In this paper, we further investigate the thermodynamic and kinetic origin of the ultrahigh glass-forming ability of this kind of HE-MG. In this letter, we explored the thermodynamic and kinetic of a non-equiautomic Ti-Zr-Ni-Cu-Be HE-MG with $\Delta S_{config} \sim 1.44R$ (R denoting the ideal gas constant) in the framework of Adam-Gibbs theory [20], and Angell's fragility [21], which shows an ultrahigh GFA with an indication of the critical size for MG above 50 mm [6], as well as excellent processability in the supercooled region and fatigue performance [22, 23]. Very strong

* Corresponding author.

E-mail address: zwzhu@imr.ac.cn (Z. Zhu).

Table 1

Thermodynamic data measured at 0.333 K/s for the TiZr-HEMG.

Compositions (at.%)	T_g (K)	T_x (K)	T_m (K)	T_l (K)	ΔT (K)	ΔH_x (kJ/mol)	ΔH_m (kJ/mol)	ΔS_m (J/(mol K))	ΔS_{config} (J/(mol K))
Ti _{32.8} Zr _{30.2} Cu ₉ Ni _{5.3} Be _{22.7}	598	651	912	942	53	3.49	5.46	5.98	11.98

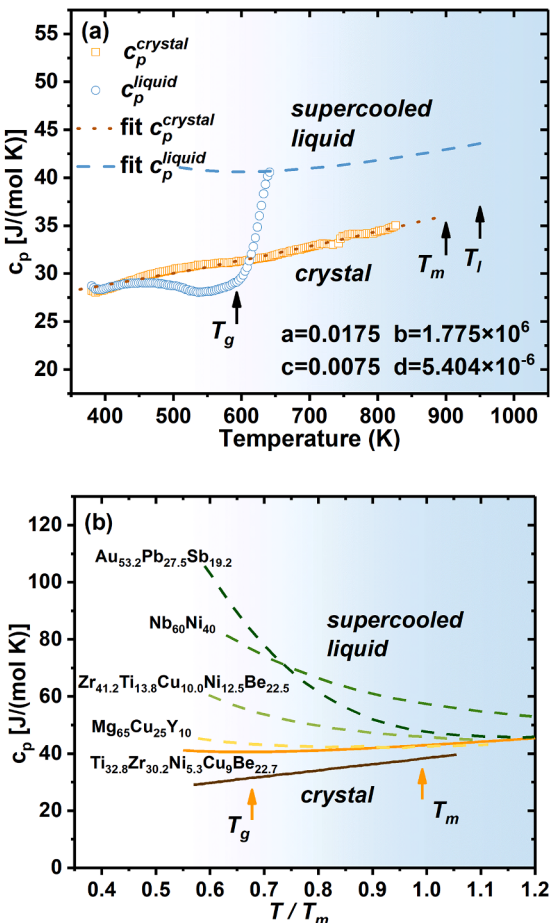


Fig. 1. (a) Specific heat capacity c_p of TiZr-HEMG in the glassy (blue dots) and crystalline (yellow squares) state with the fitted dashed and dotted lines by Eqs. (2) and (3), respectively. (b) The T/T_m dependence of specific heat capacities, c_p ($J/(mol K)$), in the supercooled liquid for several alloys [28–30].

behaviors of supercooled liquid and small Gibbs free energy difference were disclosed to be responsible for ultrahigh GFA for this non-equiautomatic HE-MG. Such findings will benefit the further interpretation of HE-MG formation mechanism thermodynamically and kinetically.

2. Experimental methods

An ingot with nominal composition of Ti_{32.8}Zr_{30.2}Ni_{5.3}Cu₉Be_{22.7} (in atomic percentage, denoted as TiZr-HEMG) was prepared by arc melting of pure elements with a purity above 99.9% in a water-cooled copper furnace under an atmosphere of titanium absorption and argon protection. The ingot was remelted and then cast into the samples with a diameter of 5 mm using a copper mold tilt-casting method. X-ray diffraction (XRD) measurements were made at the Rigaku D/max-2400 diffractometer with monochromated Cu K α radiation. The specific heat capacity were measured by using a power-compensated differential scanning calorimeter (DSC, NETZSCH 404) with standard procedure. The empty graphite pans were heated at a heating rate of 0.33 K/s to 373 K and hold for 15 min, and then heated at a heating rate of 0.33 K/s to 1223 K and hold the temperature for 10 min to obtain the baseline.

The amorphous sample, crystallized sample and a sapphire reference were heated using the above same procedure. The specific heat of amorphous and crystallized samples was accordingly calculated using the following equation (Eq. (1)):

$$c_p(T)_{\text{metal}} = \frac{\dot{Q}_{\text{metal}} - \dot{Q}_{\text{pan}}}{\dot{Q}_{\text{sapphire}} - \dot{Q}_{\text{pan}}} \frac{m_{\text{sapphire}} \cdot \mu_{\text{metal}}}{m_{\text{metal}} \cdot \mu_{\text{sapphire}}} \cdot c_p(T)_{\text{sapphire}} \quad (1)$$

in which, m_i is the mass, μ_i is the molar mass and $c_p(T)_{\text{sapphire}}$ is the specific heat capacity of the sapphire. The onset and completion of the glass transition temperature (for kinetic fragility) or the peak temperature of the first crystallization peak $T_{x1,p}$ (for activation energy) were measured with a power-compensated differential scanning calorimeter (Perkin-Elmer DSC7) through heating initially glassy samples at different heating rates containing 1, 5, 10, 20, 40, 60, 80, 100, 120, 140, 160 and 180 K/min. Aluminum sample pans were used to heat the samples up to 853 K. Argon gas purge was used for all measurements. Before measurements, the temperature and enthalpy calibration were conducted for both DSC instruments.

3. Results and discussion

3.1. Thermodynamics

Glass transition, crystallization and melting events were characterized at a heat rate of 0.333 K/s. The DSC curve is not shown herein. The alloy exhibits the apparent glass transition, followed by three crystallization events and melting. The corresponding thermal parameters including onset glass transition (T_g), onset crystallization temperature (T_x), solidus temperature (T_m), liquidus temperature (T_l), supercooled liquid region (ΔT), crystallization enthalpy (ΔH_x), and melting enthalpy (ΔH_m), etc., are summarized in Table 1. The melting entropy (ΔS_m) can then be calculated as $\Delta S_m = \Delta H_m/T_m$. As a comparison, ΔS_{config} is also listed in Table 1.

Fig. 1(a) displays the temperature dependence of specific heat capacity (c_p) of TiZr-HEMG. At relatively low temperature below ~ 450 K, c_p of the amorphous phase is similar to that of the crystalline phases. With further heating above T_g , the alloy changes from amorphous state to supercooled liquid state, and c_p of the supercooled liquid increases to a peak value of 40.7 J/(mol K). The c_p value of the supercooled liquid is reasonable compared with other BMG forming alloys [20]. At higher temperature, no c_p data of the supercooled liquid can be observed in Fig. 1(a) because of its destabilization into the crystalline products.

Based on works reported by Kubaschewski *et al.* [24], the temperature dependence of the specific heat of the supercooled liquid (c_p liquid), and the specific heat of the crystal (c_p crystal) far above the Debye temperature can be expressed as Eqs. (2) and (3), respectively, which are described in the following:

$$c_p \text{ liquid} = 3R + aT + bT^{-2} \quad (2)$$

$$c_p \text{ crystal} = 3R + cT + dT^2 \quad (3)$$

where R is the general gas constant and its value is 8.314 J/g mol, T is temperature, and a , b , c and d are the fitting parameters.

For c_p crystal, the measured results are shown in Fig. 1(a), and the corresponding fitting curve using Eq. (3) is also illustrated with the dot line. However, for c_p liquid, the only one value of c_p liquid, i.e., $c_p^{T=648K} \sim 40.7$ J/(mol K), was obtained in the current work, and thus, Eq. (2) cannot be applied without further data input [25–27].

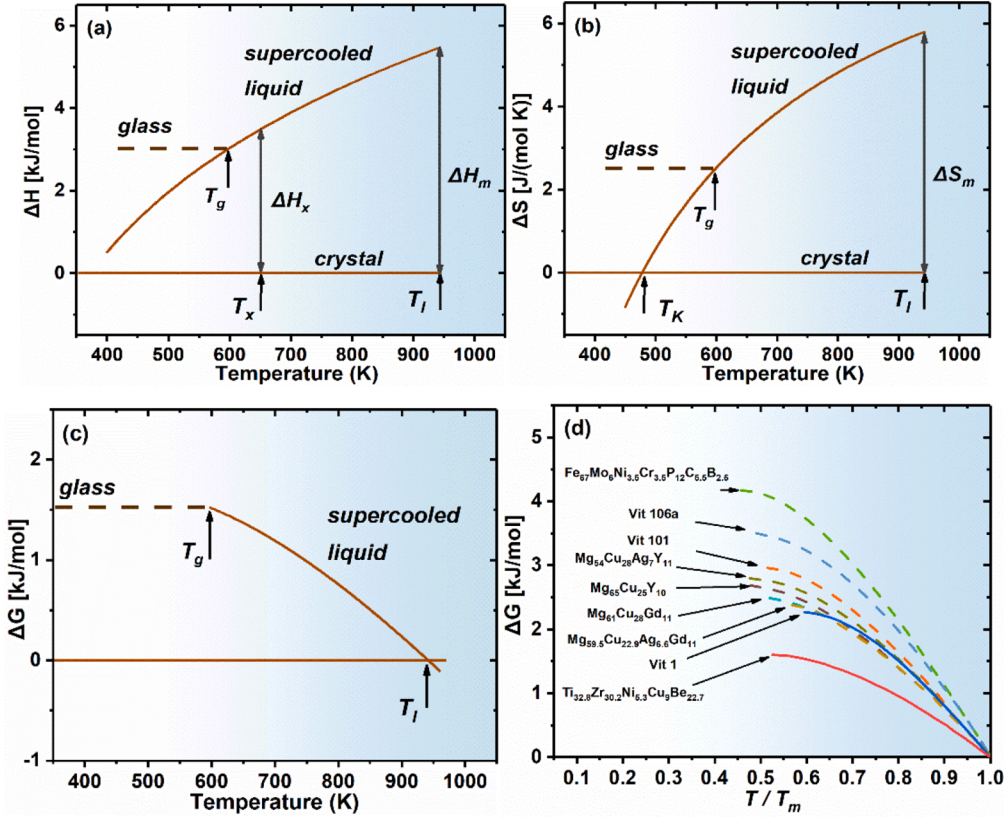


Fig. 2. (a) Enthalpy difference between the liquid and crystalline states, (b) Entropy difference between the liquid and crystalline states, (c) Gibbs free energy difference between the liquid and crystalline states as a function of temperature. (d) Gibbs free energy curves normalized by T_m comparing the present TiZr-HEMG with a series of alloys with different GFA [25, 27, 31–33].

According to Eq. (4) described in the following:

$$\Delta H_m - \Delta H_x = \int_{T_x}^{T_m} \Delta c_p^{l-x}(T') dT' \quad (4) \text{ where } \Delta c_p^{l-x} = c_p^{\text{liquid}} - c_p^{\text{crystal}}. \Delta c_p^{l-x} \text{ is}$$

connected with the difference between ΔH_m and ΔH_x [27].

Using data in Table 1, the fitting parameters of a and b were calculated by combining Eqs. (2) and (4). Finally, the estimation of the temperature dependence of c_p^{liquid} can be obtained, as shown with the dash line in Fig. 1(a).

GFA of the supercooled liquid is closely related to its Gibbs free energy, which can be calculated using c_p^{liquid} . Fig. 1(b) compares the temperature dependence of c_p^{liquid} for different glass-forming supercooled melts [28–30]. For comparison, the curve of $c_p^{\text{crystal}} \sim T$ is also shown, which stands for all the shown alloys because c_p^{crystal} varies very slightly at the same temperature for all the crystalline parts. It is clearly shown that c_p^{liquid} is higher than that of the crystalline counterparts and increases with the degree of supercooling. The curves of $c_p^{\text{liquid}} \sim T$ seems flat for good glass-forming alloys including Vit 1 and Mg₆₅Cu₂₅Y₁₀, etc.. Amongst all the shown alloys, the present TiZr-HEMG exhibits the $c_p^{\text{liquid}} \sim T$ curve closest to the $c_p^{\text{crystal}} \sim T$ one, indicating that the current alloy possesses the strongest stability against crystallization [30].

It is generally considered that the glass formation is a process to keep from crystallization. Accordingly, the thermodynamic driving force for crystallization is approximated by the Gibbs free energy difference (ΔG_{l-x}) between supercooled liquid state and crystalline state [30], which can be calculated as:

$$\Delta G_{l-x} = \Delta H_{l-x} - T \Delta S_{l-x} \quad (5)$$

where, ΔH_{l-x} and ΔS_{l-x} are the enthalpy and entropy difference between liquid state and crystal state, respectively, and can be calculated by Eqs.

(6) and (7):

$$\Delta H_{l-x} = \Delta H_m - \int_{T_x}^{T_l} \Delta c_p^{l-x}(T') dT' \quad (6)$$

$$\Delta S_{l-x} = \Delta S_m - \int_{T_x}^{T_l} \frac{\Delta c_p^{l-x}(T')}{T'} dT' \quad (7)$$

Figs. 2(a)–(c) show the variation of ΔH_{l-x} , ΔS_{l-x} and ΔG_{l-x} with temperature, respectively. With lowering the temperature, ΔH_{l-x} and ΔS_{l-x} show the typical descent behavior. The Kauzmann temperature (T_k) is the lower bound for the glass transition on account of thermodynamic reasons [28] and determined to be around 460 K in Fig. 2(b). ΔG_{l-x} rises with an increase in the supercooling. At T_k , ΔG_{l-x} is calculated to be about 1.6 kJ/mol, which is much smaller than that of Vit 1, meaning the stability of the supercooled liquid to some extent. The slope of $\Delta G_{l-x} \sim T$ curve at the melting point is determined by the fusion entropy. For the present TiZr-HEMG, it is calculated as about 5.98 J/(K mol), quite smaller than that of most of the reported glass-forming alloys, i.e., 8.75 J/(K mol) for Vit 1. The existence of strong short-range ordering is implied in the supercooled liquid, which lowers ΔG_{l-x} and enhances the glass formation. Furthermore, the $\Delta G_{l-x} \sim T$ curves are present in Fig. 2(d) to qualitatively compare GFA of different glass-forming alloys [25, 27, 31–33]. The temperature axis is normalized by T_m to allow an overall comparison. This non-equiautomic HEMG shows the lowest ΔG_{l-x} among all the alloys, that is to say, the highest GFA from a thermodynamic viewpoint. It agrees well with the fact that the current TiZr-HEMG can be cast into at least 50mm-size glassy samples [6].

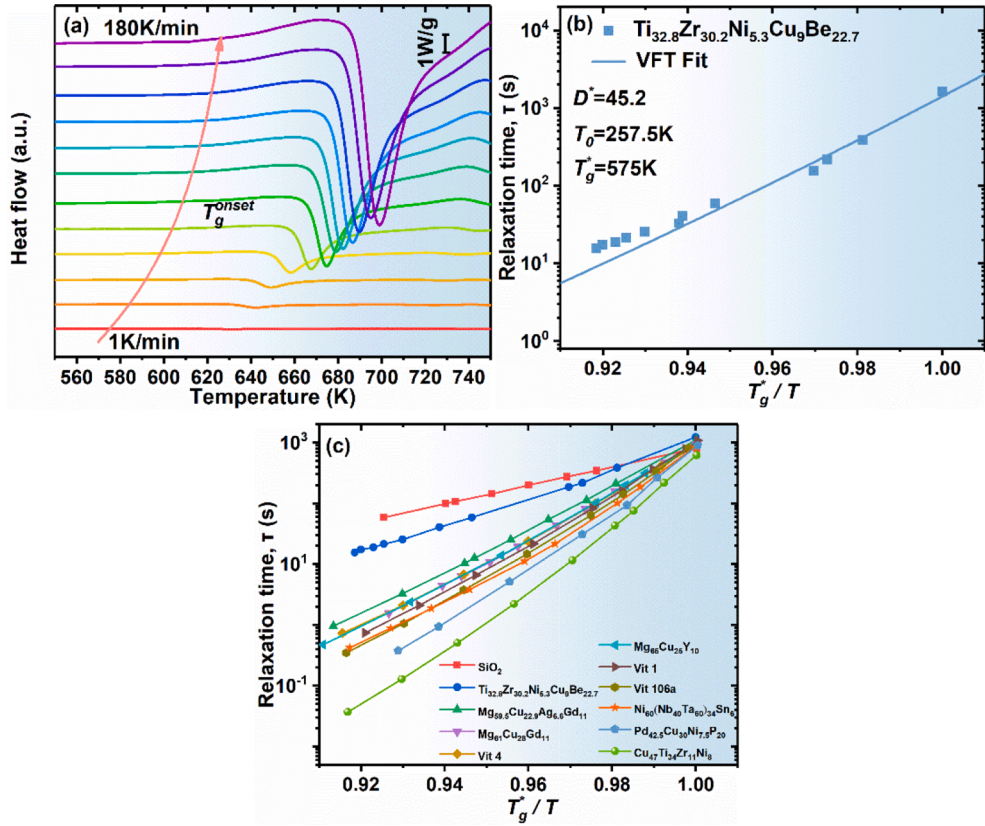


Fig. 3. (a) DSC heat flow curve of the Ti_{32.8}Zr_{30.2}Ni_{5.3}Cu₉Be_{22.7} alloy at different heating rates of 1 ~ 180 K/min, (b) the VFT fitting to $\tau \sim T_g^*/T$ dependence of Ti_{32.8}Zr_{30.2}Ni_{5.3}Cu₉Be_{22.7} alloy, (c) Angell plot near T_g^* comparing the present TiZr-HEMG with a series of alloys with different GFA [8, 29, 37-43].

3.2. Kinetics

Kinetically, the fragility concept proposed by Angell [21] describes deviations from Arrhenius temperature dependence of viscosity or relaxation time. Herein, the relaxation time was estimated using DSC measurements. T_g^{onset} and T_g^{end} are defined as the onset and end temperature of calorimetric glass transition event. At a constant heating rate (H), the average relaxation time (τ) of glass transition can be estimated by

$$\tau = \frac{T_g^{\text{end}} - T_g^{\text{onset}}}{H} = \frac{\Delta T_g}{H}. \quad (8)$$

Generally, the onset of T_g is used to approximate the temperature that corresponds to τ . The relationship between T_g and τ can be described using Vogel–Fulcher–Tammann (VFT) equation

$$\tau = \tau_0 \exp\left(\frac{D^* \cdot T_0}{T_g - T_0}\right), \quad (9) \text{ where, } D^* \text{ is the fragility index, } T_0 \text{ is the VFT}$$

temperature and τ_0 is a constant. Both D^* and T_0 are fitting parameters. At $D^* \geq 100$, the behavior is very much like Arrhenius and with D^* decreasing to below 10, the behaviors become more fragile. For MG formers, D^* is 10 ~ 35 [26]. T_0 is the temperature at which the relaxation time would go to infinity.

To obtain D^* and T_0 , τ is firstly determined using Eq. (8) at a particular heating rate. Fig. 3(a) shows the DSC curves of Ti_{32.8}Zr_{30.2}Ni_{5.3}Cu₉Be_{22.7} HEMG at different heating rates of 1 ~ 180 K/min. Both T_g^{onset} and T_g^{end} clearly shift to higher temperature for the higher heating rate, indicating the kinetic nature of glass transition [34]. In the VFT fitting, τ_0 is treated as a constant, which represents the relaxation time in the maximum limit of T , and $\tau_0 \propto N_A/hV_m$, where N_A is Avogadro's constant, h is Planck's constant, and V_m is the molar volume of the alloy [35]. The value of N_A/hV_m for Ti_{32.8}Zr_{30.2}Ni_{5.3}Cu₉Be_{22.7} HE-MG is approximately 4×10^{-5} Pa·s similar to Pt_{57.3}Cu_{14.6}Ni_{5.3}P_{22.8} alloy [36].

Consequently, the value of τ_0 for Ti_{32.8}Zr_{30.2}Ni_{5.3}Cu₉Be_{22.7} alloy is 2×10^{-13} s. In Fig. 3(b), the relaxation time is plotted with T_g^*/T , and the VFT fitting parameters obtained by a nonlinear curve fitting are also shown. The best fitting values of D^* and T_0 are found to be 45.2 and 257.5 K, respectively. As aforementioned, D^* for the present TiZr-HEMG is much higher than that for other MG formers, implying that the TiZr-HEMG shows very strong behavior in the supercooled liquid.

The Angell plots for the TiZr-HEMG together with a number of typical MG formers are shown in Fig. 3(c). D^* is about 20 for good MG formers such as Vit 1 [29,44] Vit 4 [29,38] and Vit 106a [8,44] etc.. In Fig. 3(c), the strongest glass former, SiO₂ ($D^* = 100$), is also illustrated as the limiting case. The linear like temperature dependence of the relaxation time is presented for the SiO₂ glass. It can be seen that our TiZr-HEMG is very close to SiO₂ glass, and becomes the strongest liquid among all the metallic glass-forming alloys based on available fragility data [29, 37-43]. It is suggested that GFA could be related to fragility, and the stronger the liquid, the better the GFA [42, 45]. The sluggish kinetics revealed for the TiZr-HEMG contributes to inhibiting the formation of the crystalline phases in the solidification. Sha et al. [10] proved that the initial crystallization phase of Ti_{32.8}Zr_{30.2}Ni_{5.3}Cu₉Be_{22.7} is icosahedral phase (i-phase). The study of Kelton et al. [46] showed that very similar short-range arrangements exist on either side of the interface between the glassy phase and icosahedral phase (i-phase) [47]. From this, it can be determined that the glassy phase in Ti_{32.8}Zr_{30.2}Ni_{5.3}Cu₉Be_{22.7} have short-range ordered arrangement similar to that in icosahedral phase. As discussed for SiO₂ glass with open network structure, it can be inferred by analogy that the strong short- or medium-range ordering (SRO or MRO) exists in the supercooled liquid of the present HEMG alloy. On the one hand, the strong SRO or MRO leads to strong behaviors due to sluggish kinetics. On the other hand, the existence of strong SRO or MRO also lowers the Gibbs free energy of the supercooled liquid, agreeing with the low melting entropy which

represents excellent glass-forming ability [48]. Both thermodynamic and kinetic factors lead to the present HEMG alloy showing the ultrahigh GFA.

In addition, the fragility index m [49–51] is used to describe the kinetic behavior of supercooled liquids at a particular T_g , and can also be calculated from:

$$m = \frac{D^* T_0 T_g}{(T_g - T_0)^2 \ln 10} \quad (10)$$

The value of m for $\text{Ti}_{32.8}\text{Zr}_{30.2}\text{Ni}_{5.3}\text{Cu}_9\text{Be}_{22.7}$ at a heating rate of 0.33 K/s is calculated as 26.1, which is closer to the strong limit ($m = 16$) than to the fragile limit ($m > 100$) [52] and quite higher than those of typical MGs with high GFA ($m = 35 - 50$, evaluated using the same procedure at the same heating rate).

Conclusions

In summary, the thermodynamics and kinetics of the non-equiautomic $\text{Ti}_{32.8}\text{Zr}_{30.2}\text{Ni}_{5.3}\text{Cu}_9\text{Be}_{22.7}$ HEMG alloy were investigated. It is revealed that the present HEMG not only show high stability of supercooled liquid and quite low thermodynamic driving force against the nucleation and growth of crystalline phases, but also exhibit the ultra-strong behavior near T_g by an indication of $D^* = 45.2$, comparable to that of SiO_2 glass. Both thermodynamic and kinetic factors could lead to the present HEMG possessing the excellent GFA. These findings will benefit the understanding of GFA origin in the HEMG alloys and development of new superior performance HEMG with good GFA.

Credit author statement

Yuanyuan Wang: Conceptualization, Methodology, Validation, Formal analysis, Investigation, Resources, Data Curation, Writing - Original Draft.

Zhengwang Zhu: Conceptualization, Methodology, Validation, Writing - Review & Editing, Supervision, Project administration, Funding acquisition.

Aimin Wang: Conceptualization, Methodology, Project administration.

Haifeng Zhang: Conceptualization, Supervision, Project administration.

Confirmation of authorship

As corresponding author, I Zhengwang Zhu, hereby confirm that: This manuscript has not been published, was not, and is not being submitted to any other journal. If presented at a conference, the conference is identified. If published in conference proceedings, substantial justification for re-publication must be presented. All necessary permissions for publication were secured prior to submission of the manuscript. I understand that the Corresponding Author is the sole contact for the Editorial process and is responsible for submissions of revisions and final approval of proofs.

Declaration of Competing Interest

The authors declare that they have no known competing financial interests or personal relationships that could have appeared to influence the work reported in this paper.

Acknowledgments

The authors acknowledge the financial support from the National Natural Science Foundation of China (Grant Nos. 52074257, 51790484), Chinese Academy of Sciences (Grant No. ZDBS-LY-JSC023), the Liao Ning Revitalization Talents Program (Grant Nos. XLYC1802078, XLYC1807062), Qingdao city (Grant No. 19-9-2-1-wz) and Science and Technology on Transient Impact Laboratory (Grant No.

6142606192208).

References

- [1] J.W. Yeh, S.K. Chen, S.J. Lin, J.Y. Gan, T.S. Chin, T.T. Shun, C.H. Tsau, S.Y. Chang, Nanostructured high-entropy alloys with multiple principal elements: novel alloy design concepts and outcomes, *Adv. Eng. Mater.* 6 (2004) 299–303.
- [2] C.J. Tong, Y.L. Chen, S.K. Chen, J.W. Yeh, T.T. Shun, C.H. Tsau, S.J. Lin, S.Y. Chang, Microstructure characterization of $\text{Al}_{x}\text{CoCrCuFeNi}$ high-entropy alloy system with multiprincipal elements, *Metall. Mater. Trans. A* 36a (2005) 881–893.
- [3] Y.J. Zhou, Y. Zhang, Y.L. Wang, G.L. Chen, Microstructure and compressive properties of multicomponent $\text{Al}-x(\text{TiVCrMnFeCoNiCu})(100-x)$ high-entropy alloys, *Mat. Sci. Eng. A-struct* 454 (2007) 260–265.
- [4] H.F. Li, X.H. Xie, K. Zhao, Y.B. Wang, Y.F. Zheng, W.H. Wang, L. Qin, In vitro and in vivo studies on biodegradable CaMgZnSrYb high-entropy bulk metallic glass, *Acta Biomater.* 9 (2013) 8561–8573.
- [5] Y. Zhang, T.T. Zuo, Z. Tang, M.C. Gao, K.A. Dahmen, P.K. Liaw, Z.P. Lu, Microstructures and properties of high-entropy alloys, *Prog. Mater. Sci.* 61 (2014) 1–93.
- [6] M.Q. Tang, H.F. Zhang, Z.W. Zhu, H.M. Fu, A.M. Wang, H. Li, Z.Q. Hu, TiZr-base bulk metallic glass with over 50mm in diameter, *J. Mater. Sci. Technol.* 26 (2010) 481–486.
- [7] K. Zhao, X.X. Xia, H.Y. Bai, D.Q. Zhao, W.H. Wang, Room temperature homogeneous flow in a bulk metallic glass with low glass transition temperature, *Appl. Phys. Lett.* 98 (2011), 141913.
- [8] X.Q. Gao, K. Zhao, H.B. Ke, D.W. Ding, W.H. Wang, H.Y. Bai, High mixing entropy bulk metallic glasses, *J. Non-cryst. Solids.* 357 (2011) 3557–3560.
- [9] A. Takeuchi, N. Chen, T. Wada, Y. Yokoyama, H. Kato, A. Inoue, J.W. Yeh, $\text{Pd}_{20}\text{Pt}_{20}\text{Cu}_{20}\text{Ni}_{20}\text{P}_{20}$ high-entropy alloy as a bulk metallic glass in the centimeter, *Intermetallics* 19 (2011) 1546–1554.
- [10] P.F. Sha, Z.W. Zhu, M.Q. Tang, H.M. Fu, Z.K. Li, H. Li, A.M. Wang, H.W. Zhang, H. F. Zhang, Z.Q. Hu, Effects of quasicrystal formation on the crystallization of $(\text{Ti}_{36.1}\text{Zr}_{33.8}\text{Ni}_{5.8}\text{Be}_{24.9})(100-x)\text{Cu}_x$ ($x = 5, 7, 9, 11, 13, 15, 17$) metallic glasses, *J. Appl. Phys.* 113 (2013), 033508.
- [11] H.Y. Ding, K.F. Yao, High entropy $\text{Ti}_{20}\text{Zr}_{20}\text{Cu}_{20}\text{Ni}_{20}\text{Be}_{20}$ bulk metallic glass, *J. Non-cryst. Solids.* 364 (2013) 9–12.
- [12] P. Gong, J.S. Jin, L. Deng, S.B. Wang, J.L. Gu, K.F. Yao, X.Y. Wang, Room temperature nanoindentation creep behavior of TiZrHfBeCu(Ni) high entropy bulk metallic glasses, *Mat. Sci. Eng. A-struct* 688 (2017) 174–179.
- [13] Y.Q. Xu, Y.H. Li, Z.W. Zhu, W. Zhang, Formation and properties of $\text{Fe}_{25}\text{Co}_{25}\text{Ni}_{25}(\text{P}, \text{C}, \text{B}, \text{Si})_{25}$ high-entropy bulk metallic glasses, *J. Non-cryst. Solids.* 487 (2018) 60–64.
- [14] W.Q. Li, Z.W. Zhu, G.J. Li, L. Zhang, Z.K. Li, H.M. Fu, H.W. Zhang, H. Li, A. M. Wang, H.F. Zhang, Correlation between dynamic compressive strength and fracture behaviors of bulk metallic glasses, *Acta Metall. Sin. - Engl.* 33 (2020) 1407–1415.
- [15] W.H. Wang, High-Entropy Metallic Glasses, *JOM* 66 (2014) 2067–2077.
- [16] Y. Chen, J.Z. Jiang, A novel strategy to design Zr-Co-Al BMG composites containing only $\text{B}_2\text{-ZrCo}$ phase, *Intermetallics* 123 (2020).
- [17] Y. Chen, J.Z. Jiang, Formation of the $\text{B}_2\text{-ZrCo}$ phase and micro-hardness evolution in Zr-Co-Al BMGs via conventional and flash annealing, *J. Alloy. Compd.* 834 (2020), 154230.
- [18] Y. Chen, C.G. Tang, J.Z. Jiang, Recent development of ZrCo -based BMGs and their composites, *J. Non-cryst. Solids.* 546 (2020), 120288.
- [19] A.L. Greer, Materials Science - Confusion by Design, *Nature* 366 (1993) 303–304.
- [20] R. Busch, J. Schroers, W.H. Wang, Thermodynamics and kinetics of bulk metallic glass, *Mrs. Bull.* 32 (2007) 620–623.
- [21] C.A. Angell, Formation of Glasses from Liquids and Biopolymers, *Science* 267 (1995) 1924–1935.
- [22] X.D. Wang, P. Liu, Z.W. Zhu, H.F. Zhang, X.C. Ren, High fatigue endurance limit of a Ti-based metallic glass, *Intermetallics* 119 (2020), 106716.
- [23] X.D. Wang, S.L. Song, P. Liu, Z.W. Zhu, H.F. Zhang, X.C. Ren, Shear band deformation and fatigue striations during three-point bending fatigue crack growth in brittle metallic glass, *J. Non-cryst. Solids.* 536 (2020), 119988.
- [24] J. Schroers, B. Lohwongwatana, W.L. Johnson, A. Peker, Gold based bulk metallic glass, *Appl. Phys. Lett.* 87 (2005), 061912.
- [25] I. Gallino, M.B. Shah, R. Busch, Enthalpy relaxation and its relation to the thermodynamics and crystallization of the $\text{Zr}_{58.5}\text{Cu}_{15.6}\text{Ni}_{12.8}\text{Al}_{10.3}\text{Nb}_{2.8}$ bulk metallic glass-forming alloy, *Acta Mater.* 55 (2007) 1367–1376.
- [26] I. Gallino, J. Schroers, R. Busch, Kinetic and thermodynamic studies of the fragility of bulk metallic glass forming liquids, *J. Appl. Phys.* 108 (2010), 063501.
- [27] B. Bochtler, O. Gross, I. Gallino, R. Busch, Thermo-physical characterization of the $\text{Fe}_{67}\text{Mn}_{9.5}\text{Cr}_{3.5}\text{P}_{12}\text{C}_{5.5}\text{B}_{2.5}$ bulk metallic glass forming alloy, *Acta Mater.* 118 (2016) 129–139.
- [28] R. Busch, Y.J. Kim, W.L. Johnson, Thermodynamics and kinetics of the undercooled liquid and the glass-transition of the $\text{Zr}_{41.2}\text{Ti}_{13.8}\text{Cu}_{12.5}\text{Ni}_{10.0}\text{Be}_{22.5}$ alloy, *J. Appl. Phys.* 77 (1995) 4039–4043.
- [29] R. Busch, E. Bakke, W.L. Johnson, Viscosity of the supercooled liquid and relaxation at the glass transition of the $\text{Zr}_{46.75}\text{Ti}_{18.25}\text{Cu}_{7.5}\text{Ni}_{10}\text{Be}_{27.5}$ bulk metallic glass forming alloy, *Acta Mater.* 46 (1998) 4725–4732.
- [30] R. Busch, The thermophysical properties of bulk metallic glass-forming liquids, *Jom - J. Min. Met. Mat. S.* 52 (2000) 39–42.
- [31] S.C. Glade, R. Busch, D.S. Lee, W.L. Johnson, R.K. Wunderlich, H.J. Fecht, Thermodynamics of $\text{Cu}_{47}\text{Ti}_{34}\text{Zr}_{11}\text{Ni}_8$, $\text{Zr}_{52.5}\text{Cu}_{17.9}\text{Ni}_{14.6}\text{Al}_{10}\text{Ti}_5$ and

- [32] I. Gallino, D. Cangialosi, Z. Evenson, L. Schmitt, S. Hechler, M. Stolpe, B. Ruta, Hierarchical aging pathways and reversible fragile-to-strong transition upon annealing of a metallic glass former, *Acta Mater.* 144 (2018) 400–410.
- [33] M. Frey, R. Busch, W. Possart, I. Gallino, On the thermodynamics, kinetics, and sub-T_g relaxations of Mg-based bulk metallic glasses, *Acta Mater.* 155 (2018) 117–127.
- [34] Q. Zheng, J. Xu, E. Ma, High glass-forming ability correlated with fragility of Mg-Cu(Ag)-Gd alloys, *J. Appl. Phys.* 102 (2007), 113519.
- [35] H.R. Jiang, B. Bochtler, S.S. Riegler, X.S. Wei, N. Neuber, M. Frey, I. Gallino, R. Busch, J. Shen, Thermodynamic and kinetic studies of the Cu-Zr-Al(-Sn) bulk metallic glass-forming system, *J. Alloy. Compd.* 844 (2020), 156126.
- [36] B.A. Legg, J. Schroers, R. Busch, Thermodynamics, kinetics, and crystallization of Pt_{57.5}Cu_{14.6}Ni_{5.3}P_{22.8} bulk metallic glass, *Acta Mater.* 55 (2007) 1109–1116.
- [37] R. Busch, W. Liu, W.L. Johnson, Thermodynamics and kinetics of the Mg₆₅Cu₂₅Y₁₀ bulk metallic glass forming liquid, *J. Appl. Phys.* 83 (1998) 4134–4141.
- [38] R. Busch, W.L. Johnson, The kinetic glass transition of the Zr_{46.75}Ti_{18.25}Cu_{7.5}Ni₁₀Be_{27.5} bulk metallic glass former-supercooled liquids on a long time scale, *Appl. Phys. Lett.* 72 (1998) 2695–2697.
- [39] S.C. Glade, W.L. Johnson, Viscous flow of the Cu₄₇Ti₃₄Zr₁₁Ni₈ glass forming alloy, *J. Appl. Phys.* 87 (2000) 7249–7251.
- [40] C.C. Hays, J. Schroers, W.L. Johnson, T.J. Rathz, R.W. Hyers, J.R. Rogers, M. B. Robinson, Vitrification and determination of the crystallization time scales of the bulk-metallic-glass-forming liquid Zr_{58.5}Nb_{2.8}Cu_{15.6}Ni_{12.8}Al_{10.3}, *Appl. Phys. Lett.* 79 (2001) 1605–1607.
- [41] N. Nishiyama, A. Inoue, Glass-forming ability of Pd_{42.5}Cu₃₀Ni_{7.5}P₂₀ alloy with a low critical cooling rate of 0.067K/s, *Appl. Phys. Lett.* 80 (2002) 568–570.
- [42] L. Shadowspeaker, R. Busch, On the fragility of Nb-Ni-based and Zr-based bulk metallic glasses, *Appl. Phys. Lett.* 85 (2004) 2508–2510.
- [43] H. Kato, T. Wada, M. Hasegawa, J. Saida, A. Inoue, H.S. Chen, Fragility and thermal stability of Pt- and Pd-based bulk glass forming liquids and their correlation with deformability, *Scripta Mater.* 54 (2006) 2023–2027.
- [44] R. Busch, A. Masuhr, E. Bakke, W.L. Johnson, Bulk metallic glass formation from strong liquids, *Mech. Alloyed, Metastab. Nanocryst. Mater., Part 2*, 269-2 (1998) 547–552.
- [45] S. Mukherjee, J. Schroers, W.L. Johnson, W.K. Rhim, Influence of kinetic and thermodynamic factors on the glass-forming ability of zirconium-based bulk amorphous alloys, *Phys. Rev. Lett.* 94 (2005), 245501.
- [46] Y.C. Kim, J.H. Na, J.M. Park, D.H. Kim, J.K. Lee, W.T. Kim, Role of nanometer-scale quasicrystals in improving the mechanical behavior of Ti-based bulk metallic glasses, *Appl. Phys. Lett.* 83 (2003) 3093–3095.
- [47] H.E. Kissinger, Variation of peak temperature with heating rate in differential thermal analysis, *J. Res. Natl. Bur. Stand.* 57 (1956) 217–221.
- [48] L.M. Wang, R.P. Liu, Y.J. Tian, On glass formation thermodynamics: enthalpy vs, Entropy, *Acta Phys Sin-Ch Ed* 69 (2020), 196401.
- [49] C.A. Angell, Spectroscopy simulation and scattering, and the medium range order problem in glass, *J. Non-cryst. Solids.* 73 (1985) 1–17.
- [50] M.D. Ediger, C.A. Angell, S.R. Nagel, Supercooled liquids and glasses, *J. Phys. Chem. Us* 100 (1996) 13200–13212.
- [51] D.N. Perera, Compilation of the fragility parameters for several glass-forming metallic alloys, *J. Phys.-condens. Mat.* 11 (1999) 3807–3812.
- [52] T.A. Waniuk, R. Busch, A. Masuhr, W.L. Johnson, Equilibrium viscosity of the Zr_{41.2}Ti_{13.8}Cu_{12.5}Ni₁₀Be_{22.5} bulk metallic glass-forming liquid and viscous flow during relaxation, phase separation, and primary crystallization, *Acta Mater.* 46 (1998) 5229–5236.